iScience

CellPress
OPEN ACCESS

Article

High-efficiency electrocatalytic nitrite reduction toward ammonia synthesis on CoP@TiO_2 nanoribbon array

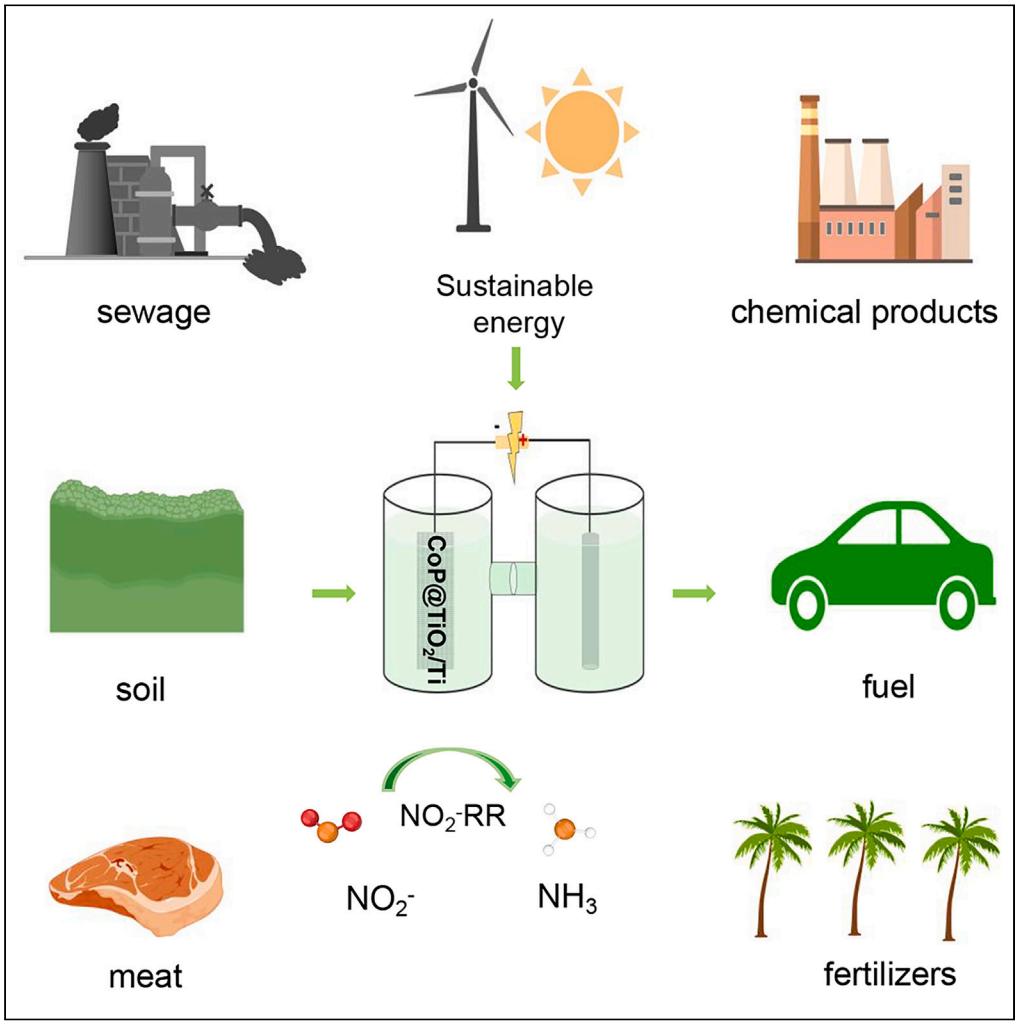

Xun He, Zixiao Li, Jie Yao, ..., Lisi Xie, Qian Liu, Xuping Sun

liuqian@cdu.edu.cn (Q.L.)
xpsun@uestc.edu.cn (X.S.)

Highlights

$CoP@TiO_2$/TP acts as a superb NO_2^-RR electrocatalyst for NH_3 synthesis

It achieves a NH_3 yield of 849.57 μmol h^{-1} cm^{-2} and a Faradaic efficiency of 97.01%

It shows good stability for 12 h of bulk electrolysis and recycling tests

The fabricated Zn–NO_2^- battery achieves a NH_3 yield of 714.40 μg h^{-1} cm^{-2}

He et al., iScience 26, 107100
July 21, 2023
https://doi.org/10.1016/j.isci.2023.107100

iScience

CellPress
OPEN ACCESS

Article

High-efficiency electrocatalytic nitrite reduction toward ammonia synthesis on CoP@TiO_2 nanoribbon array

Xun He,[1,2] Zixiao Li,[2] Jie Yao,[2] Kai Dong,[2] Xiuhong Li,[2] Long Hu,[2] Shengjun Sun,[3] Zhengwei Cai,[3] Dongdong Zheng,[3] Yongsong Luo,[2] Binwu Ying,[2] Mohamed S. Hamdy,[4] Lisi Xie,[1] Qian Liu,[1,*] and Xuping Sun[2,3,5,*]

SUMMARY

Electrochemical reduction of nitrite (NO_2^-) can satisfy the necessity for NO_2^- contaminant removal and deliver a sustainable pathway for ammonia (NH_3) generation. Its practical application yet requires highly efficient electrocatalysts to boost NH_3 yield and Faradaic efficiency (FE). In this study, CoP nanoparticle-decorated TiO_2 nanoribbon array on Ti plate (CoP@TiO_2/TP) is verified as a high-efficiency electrocatalyst for the selective reduction of NO_2^- to NH_3. When measured in 0.1 M NaOH with NO_2^-, the freestanding CoP@TiO_2/TP electrode delivers a large NH_3 yield of 849.57 μmol h^{-1} cm^{-2} and a high FE of 97.01% with good stability. Remarkably, the subsequently fabricated Zn–NO_2^- battery achieves a high power density of 1.24 mW cm^{-2} while delivering a NH_3 yield of 714.40 μg h^{-1} cm^{-2}.

INTRODUCTION

Ammonia (NH_3) is a vital chemical feedstock in the manufacturing of fertilizers, explosives, rubber, etc., and is deemed as a fascinating next-generation energy supply source for non-carbon fuel cell.[1–4] Presently, industrial massive synthesis of NH_3 counts on the Haber-Bosch method, which yet suffers from numerous energy consumption and global carbon oxide emissions.[5,6] In this regard, lots of effort have been focused on electrochemical nitrogen reduction reaction (NRR) in aqueous media, but NRR is a gas-liquid-solid reaction with low nitrogen solubility (6.8×10^{-4} M in water) that many catalysts are not ideal for nitrogen adsorption and cleavage and have low overpotential for hydrogen evolution reaction, which seriously hinders the activity and selectivity.[7–18] Nitrite (NO_2^-), in contrast, is a highly water-soluble compound with weak N=O bond (204 kJ mol^{-1}).[19,20] It is not only generally found in soil and sewage but commonly applied in curing meat products, and its extreme accumulation poses environment and human health hazards.[21,22] Encouragingly, electrochemical NO_2^- reduction not only eliminates NO_2^- pollutants but also yields NH_3, but this process involves a six-electron transfer process that requires high-efficiency NO_2^- reduction reaction (NO_2^-RR) catalysts to generate NH_3.[23,24]

Precious metal-based catalysts are active toward NO_2^-RR, but their scarcity and high cost severely hinder their application.[25–28] Earth-abundant and low-budget non-precious alternatives are therefore very attractive.[29–35] In particular, CoP has attracted increasing interest for its high conductivity and operational persistence, as well as outstanding H-adsorbing ability for catalytic hydrogenation reactions,[36,37] and has been confirmed to have NO_2^-RR activity.[38,39] Recent studies have also verified that TiO_2, which has the merits of being non-toxic, chemically stable, and structurally stable, is commonly applied to disperse highly reactive metal-based materials.[40–43] TiO2 is active toward the NO_2^-RR, and its catalytic efficiency can be further improved by P or V doping.[19,44,45] We thus believe that CoP@TiO_2 composite can effectively catalyze the NO_2^--to-NH_3 conversion, which however has not been addressed so far.

Herein, we present our recent experiment results that CoP nanoparticle-decorated TiO_2 nanoribbon array supported on Ti plate (CoP@TiO_2/TP) serves as a superb NO_2^-RR catalyst for ambient NH_3 electrosynthesis with excellent selectivity. When tested in alkaline environments, CoP@TiO_2/TP attains an extraordinary NH_3 yield of 849.57 μmol h^{-1} cm^{-2} and a high NH_3 Faradaic efficiency (FE) of 97.01%. Furthermore, we demonstrated a Zn–NO_2^- battery with CoP@TiO_2/TP cathode has high power density as well as generating satisfying NH_3 yield.

[1]Institute for Advanced Study, Chengdu University, Chengdu, Sichuan 610106, China

[2]Institute of Fundamental and Frontier Sciences, University of Electronic Science and Technology of China, Chengdu, Sichuan 610054, China

[3]College of Chemistry, Chemical Engineering and Materials Science, Shandong Normal University, Jinan, Shandong 250014, China

[4]Catalysis Research Group (CRG), Department of Chemistry, College of Science, King Khalid University, P.O. Box 9004, 61413 Abha, Saudi Arabia

[5]Lead contact

*Correspondence: liuqian@cdu.edu.cn (Q.L.), xpsun@uestc.edu.cn (X.S.)

https://doi.org/10.1016/j.isci.2023.107100

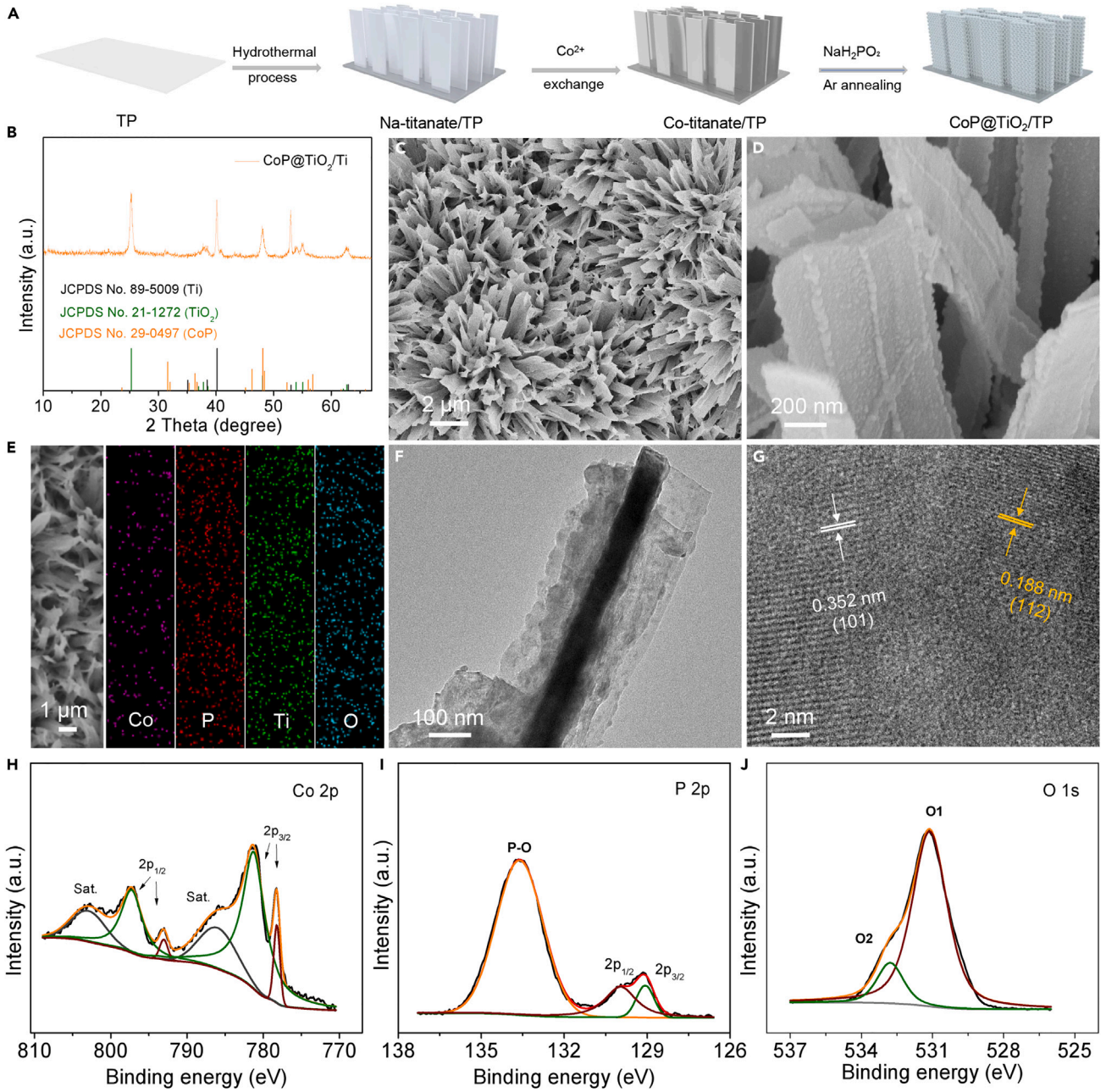

Figure 1. Structural characteristics of CoP@TiO_2/TP

(A) Schematic diagram of the fabrication process of CoP@TiO_2/TP.

(B) XRD pattern of CoP@TiO_2/TP.

(C) Low- and (D) high-magnification SEM images of CoP@TiO_2/TP.

(E) SEM and corresponding EDX elemental mapping images of CoP@TiO_2.

(F) TEM and (G) HRTEM images of CoP@TiO_2.

(H–J) High-resolution XPS spectra of CoP@TiO_2 in the (H) Co 2p, (I) P 2p, and (J) O 1s regions.

RESULTS AND DISCUSSION

As depicted in Figure 1A, CoP@TiO_2/TP was fabricated via hydrothermal process, Co^{2+} exchange, and Ar annealing phosphorylation. Figures 1B and S1 exhibit the X-ray diffraction pattern of CoP@TiO_2/TP and TiO_2/TP, which both display the diffraction peak features of TiO_2 (JCPDS No. 21–1272) and Ti (JCPDS No. 89–5009), while the remaining peaks of CoP@TiO_2/TP are assigned to CoP (JCPDS No. 29–0497).

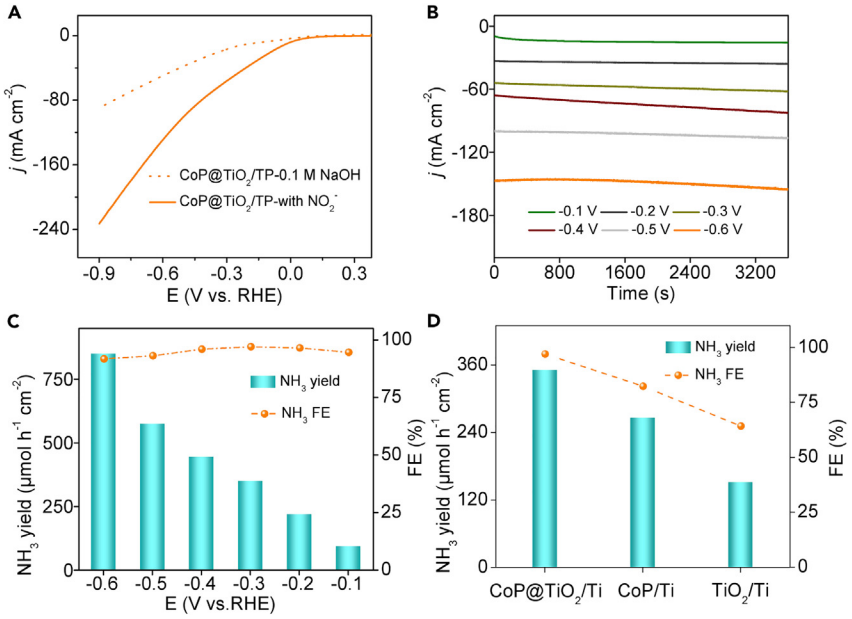

Figure 2. Electrochemical NO_2^-RR tests

(A) LSV curves of CoP@TiO_2/TP in 0.1 M NaOH with/without 0.1 M NO_2^-.

(B) CA curves of CoP@TiO_2/TP at various potentials.

(C) NH_3 yields and FEs of CoP@TiO_2/TP at various potentials.

(D) Comparison of NH_3 yield and FE of CoP@TiO_2/TP, CoP/TP, and TiO_2/TP at −0.3 V.

The SEM images in Figures S2 and S3 exhibit that TP is fully covered by TiO_2 nanoribbon array. And SEM (Figures 1C and 1D) and transmission electron microscopy (TEM) (Figure 1F) images indicate that CoP nanoparticle precipitated from the interlayer of TiO_2 during the phosphorylation reaction and were embedded on the surface of TiO_2 nanoribbon array. The SEM and corresponding energy-dispersive X-ray elemental mapping images (Figure 1E) of CoP@TiO_2 reveal the even element distribution of Co, P, Ti, and O, and the mass percentage of CoP in CoP@TiO_2 is approximately 28.92% (Figure S4). Furthermore, the high-resolution TEM image of CoP@TiO_2 (Figure 1G) validates lattice spacings of 0.188 and 0.352 nm, ascribed to the (112) and (101) crystal surfaces of CoP and TiO_2, respectively. It is therefore reasonable to infer we have successfully prepared CoP nanoparticle-decorated TiO_2 nanoribbon array supported on TP. Besides that, the X-ray photoelectron spectroscopy (XPS) spectrum was applied to study the surface chemical compositions of CoP@TiO_2. As shown in Figure 1H, the XPS spectrum of CoP@TiO_2 in Co 2p region is divided into six peaks. The peaks at the binding energies (BEs) of 797.25 and 793.04 eV are assigned to Co $2p_{1/2}$, and the peaks at the BEs of 781.25 and 778.21 eV match with Co $2p_{3/2}$, while the peaks at the BEs of 802.94 and 785.99 eV are assigned to two satellites (defined as "Sat."). [37,46] In the P 2p region (Figure 1I), three peaks at the BEs of 133.61, 129.07, and 129.96 eV are associated with P-O, P $2p_{1/2}$, and P $2p_{3/2}$, respectively. [37,47] In the Ti 2p region (Figure S5), two peaks at the BEs of 458.87 and 464.69 eV are attributed to Ti $2p_{3/2}$ and Ti $2p_{1/2}$, respectively. [48] Besides, the O 1s region spectrum was fitted to two peaks, located at the BEs of 531.12 and 532.78 eV, ascribed to the metal-oxygen bond (O_1) and the lattice oxygen (O_2), respectively (Figure 1J). [48,49]

The electrocatalytic activity of NO_2^-RR was evaluated in 0.1 M NaOH electrolyte with 0.1 M NO_2^-. The indophenol blue and the Watt and Crisp method were used to count NH_3 and the potential by-product of N_2H_4 (Figures S6 and S7), respectively. Figures 2A and S8 present the linear scanning voltammetry (LSV) curves of CoP@TiO_2/TP, CoP/TP, and TiO_2/TP. It is obvious that CoP@TiO_2/TP delivers a larger current density (*j*) once NO_2^- is added, which reveals that CoP@TiO_2/TP can catalyze the reduction of NO_2^- effectively. Comparatively, TiO_2/TP and CoP/TP with the presence of NO_2^- show a lower *j*. We then performed chronoamperometry tests to investigate NH_3 yields and FEs from −0.1 to −0.6 V (Figure 2B). It unveils more NH_3 is formed as the cathodic potential rises (Figure S9). Notably, the FEs of CoP@TiO_2/TP are high at each potential (over 90%) and the highest value of 97.01% occurred at −0.3 V with a corresponding NH_3 yield of 350.87 μmol h^{-1} cm^{-2}. And such CoP@TiO_2/TP achieved a superb

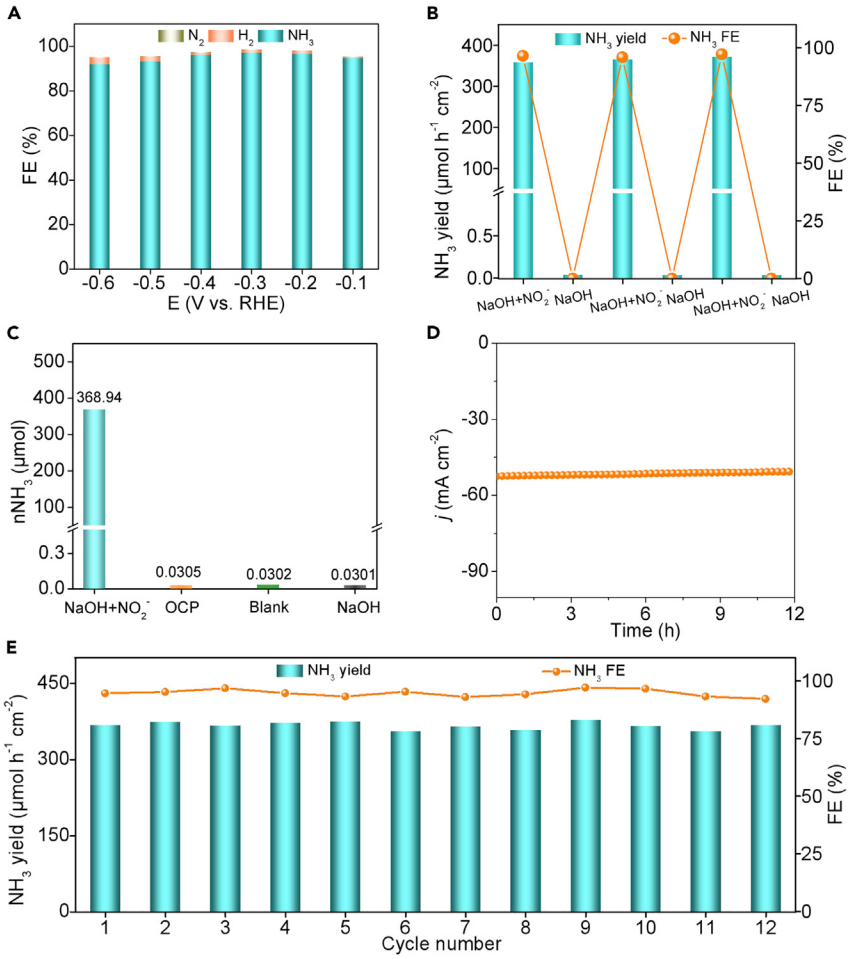

Figure 3. By-product analysis and stability tests of CoP@TiO_2/TP toward NO_2^-RR

(A) FEs of H_2, N_2, and NH_3 for CoP@TiO_2/TP at different potentials.

(B) NH_3 yields and FEs of CoP@TiO_2/TP during the alternating cycling tests.

(C) NO_2^-RR performance of CoP@TiO_2/TP under different test conditions.

(D) Time-dependent current density curve during 12-h electrolysis of CoP@TiO_2/TP at −0.3 V.

(E) Recycling tests of CoP@TiO_2/TP at −0.3 V.

NH_3 yield of 849.57 μmol h^{-1} cm^{-2} at −0.6 V. It is notable that the electrocatalytic activity of CoP@TiO_2/TP exceeds that of most the already reported NO_2^-RR catalysts mentioned in Table S1. Synchronously, the NO_2^--to-NH_3 transformation of CoP/TP and TiO_2/TP was measured at −0.3 V. As shown in Figure 2D, CoP@TiO_2/TP obviously showed better electrocatalytic activity than that of CoP/TP (82.3%, 266.15 μmol h^{-1} cm^{-2}) and TiO_2/TP (64.2%, 151.46 μmol h^{-1} cm^{-2}). The outstanding NH_3-producing ability of CoP@TiO_2/TP is attributed to two main factors. Firstly, the self-supported CoP@TiO_2/TP electrode eliminates the need for a polymer binder, thus enhancing electrode dynamics. Secondly, the readily available TiO_2 array with its unique nanoribbon-like structure provides a large specific surface area that improves the dispersibility of CoP nanoparticle and prevents its agglomeration, thus enhancing the adsorption ability of NO_2^-.

The catalytic process of CoP@TiO_2/TP was following evaluated by identifying diverse by-products (H_2, N_2H_4, and N_2) in the complex pathway from NO_2^- to NH_3. Of note, we found that CoP@TiO_2/TP did not produce N_2H_4 toward NO_2^-RR process (Figure S10). And the partial current density and FEs of the gas-phase H_2 and N_2 at the entire potential window were nearly negligible (Figures S11 and 3A), affirming great NO_2^-RR selectivity of CoP@TiO_2/TP toward NH_3 synthesis. We then performed alternating electrolysis at −0.3 V between NO_2^--containing and NO_2^--free solution for 6 cycles. It is obvious that NH_3 was yielded

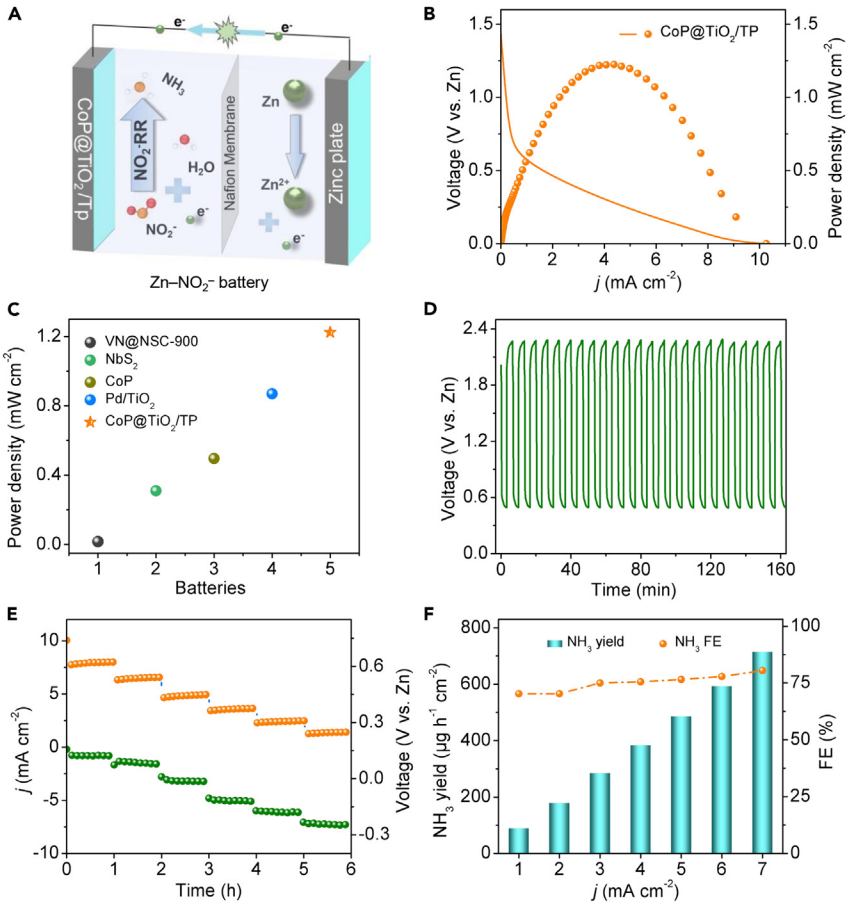

Figure 4. Zn–NO_2^- battery with CoP@TiO_2/TP cathode

(A) Schematic illustration of the Zn–NO_2^- battery.

(B) Discharge curve and the resultant power density curve of the battery.

(C) Comparison of power density for the current Zn–NO_2^- battery with CoP@TiO_2/TP as the cathode with the reported Zn–N_2, Zn–NO, and Zn–NO_3^- batteries.

(D) Charge–discharge voltage profiles of the Zn–NO_2^- battery at 2 mA cm^{-2}.

(E) Discharging tests at various current densities.

(F) NH_3 yields and FEs at different current densities.

only in the solution containing NO_2^- (Figure 3B). And it can be further seen from Figures 3C and S12 that extremely small quantity of NH_3 (all less than 0.04) was generated by electrolysis for 1 h in open circuit potential, blank solution, and NO_2^--free NaOH electrolyte, which uncovers ammonia just derived from CoP@TiO_2/TP, eliminating electrolyte and equipment interferences. Besides, we confirmed the long-lasting tolerance of CoP@TiO_2/TP by electrolysis at −0.3 V for 12 h (*j* decreased by only 2%) (Figure 3D). Also, the NH_3 yield and FE did not change much for 12 electrolysis cycles (Figures 3E and S13), indicating the outstanding repeatability of CoP@TiO_2/TP for the ambient electroreduction of NO_2^- to NH_3. Significantly, the LSV curve (Figure S14), composition (Figure S15), and morphology (Figure S16) of CoP@TiO_2/TP remain almost identical even after 12-h electrolysis. Those suggest the exceptional stability of CoP@TiO_2/TP for NH_3 generation by NO_2^-RR under working conditions.

Zn–NO_2^- battery is capable of releasing energy with a theoretical voltage of 1.59 V and can provide a high power density of 964 Wh kg^{-1} while producing value-added NH_3.[34] Based on the previous analysis that CoP@TiO_2/TP has been verified as a high-efficiency NO_2^-RR catalyst toward NH_3 synthesis, we thus assembled the CoP@TiO_2/TP-based Zn–NO_2^- battery (Figure 4A). The performance of the fabricated battery was initially evaluated by a discharge curve, which showed an increase in output *j* when the cathode potential became more negative, and reached the maximum power density of 1.22 mW cm^{-2} (Figure 4B), higher than

the reported aqueous Zn–N_2, Zn–NO, and Zn–NO_3^- batteries (Figure 4C).[47,50–52] As exhibited in Figure 4D, the charge/discharge voltage profiles of such battery at 2 mA cm^{-2} displayed only slight deviations, which confirm the potential rechargeability of our battery. Besides, Figure 4E presents the discharging curves of the fabricated battery with various *j* for 1 h and the *j* increased gradually from 1 mA cm^{-2}, reaching 7 mA cm^{-2} at approximate 0.25 V vs. Zn^{2+}/Zn, demonstrating superior electrochemical performance and long-lasting stability. The NH_3 yields and FEs of the CoP@TiO_2/TP-based Zn–NO_2^- battery were next measured as shown in Figure 4F. As expected, the FEs of NH_3 production were appealing at various *j* and it shows a high FE of 80.45% with a NH_3 yield of 714.4 μg h^{-1} cm^{-2} at a *j* of 7 mA cm^{-2}. Therefore, a NO_2^--containing energy conversion device involving NO_2^-RR is potential for applications.

Conclusions

In summary, CoP@TiO_2/TP is experimentally proved to be a high-efficiency NO_2^-RR electrocatalyst for NH_3 production under ambient conductions, which is capable of yielding a large NH_3 yield of 849.57 μmol h^{-1} cm^{-2} and a high FE of 97.01% with a long electrolytic durability. Impressively, the fabricated Zn–NO_2^- battery obtains a remarkable power density of 1.22 mW cm^{-2} with a large NH_3 yield of 714.4 μg h^{-1} cm^{-2} by utilizing CoP@TiO_2/TP as a cathode, and it shows potential rechargeability. This work provides us with an earth-abundant catalyst material for ambient NH_3 electrosynthesis and other applications.

Limitations of the study

A CoP@TiO_2/TP-based Zn–NO_2^- battery presents a "killing three birds with one stone" strategy, providing energy supply, ammonia generation, and removal of pollutants. At the moment, however, it does not seem to be a good battery or ammonia synthesis device, hindering by its low ammonia yield and power density. In the future, research efforts will focus on developing cathode materials that can produce high ammonia yield and power density, as well as investigating the reactions that occur on the cathode during charging.

STAR★METHODS

Detailed methods are provided in the online version of this paper and include the following:

- KEY RESOURCES TABLE
- RESOURCE AVAILABILITY
  - Lead contact
  - Materials availability
  - Data and code availability
- METHOD DETAILS
  - Synthesis of CoP@TiO_2/TP
  - Characterizations
  - Electrochemical measurements

SUPPLEMENTAL INFORMATION

Supplemental information can be found online at https://doi.org/10.1016/j.isci.2023.107100.

ACKNOWLEDGMENTS

The authors extend their appreciation to the Deanship of Scientific Research at King Khalid University for funding support through large group Research Project under Grant No. RGP2/199/44.

AUTHOR CONTRIBUTIONS

X.H. and Z.L. performed experiments. X.H., Z.L., J.Y., K.D., X.L., L.H., S.S., Z.C., D.Z., Y.L., B.Y., M.S.H., L.X., Q.L., and X.S. carried out data analysis and discussion. Q.L. and X.S. designed this study and wrote the paper.

DECLARATION OF INTERESTS

The authors declare no competing interests.

Received: March 28, 2023
Revised: April 20, 2023
Accepted: June 8, 2023
Published: June 14, 2023

REFERENCES

1. Liang, J., Liu, Q., Alshehri, A.A., and Sun, X. (2022). Recent advances in nanostructured heterogeneous catalysts for N-cycle electrocatalysis. Nano Res. Energy *1*, e9120010. https://doi.org/10.26599/NRE.2022.9120010.

2. Jain, M., Muthalathu, R., and Wu, X.Y. (2022). Electrified ammonia production as a commodity and energy storage medium to connect the food, energy, and trade sectors. iScience *25*, 104724. https://doi.org/10.1016/j.isci.2022.104724.

3. Zhao, Y., Liu, Y., Zhang, Z., Mo, Z., Wang, C., and Gao, S. (2022). Flower-like open-structured polycrystalline copper with synergistic multi-crystal plane for efficient electrocatalytic reduction of nitrate to ammonia. Nano Energy *97*, 107124. https://doi.org/10.1016/j.nanoen.2022.107124.

4. Qi, D., Lv, F., Wei, T., Jin, M., Meng, G., Zhang, S., Liu, Q., Liu, W., Ma, D., Hamdy, M.S., et al. (2022). High-efficiency electrocatalytic NO reduction to NH_3 by nanoporous. Nano Res. Energy *1*, e9120022. https://doi.org/10.26599/NRE.2022.9120022.

5. Kandemir, T., Schuster, M.E., Senyshyn, A., Behrens, M., and Schlögl, R. (2013). The Haber–Bosch process revisited: on the real structure and stability of "ammonia iron" under working conditions. Angew. Chem. Int. Ed. Engl. *52*, 12723–12726. https://doi.org/10.1002/anie.201305812.

6. Dybkjaer, I. (1995). Ammonia Production Processes (Springer), pp. 199–308. https://doi.org/10.1007/978-3-642-79197-0_6.

7. Chu, K., Li, X., Li, Q., Guo, Y., and Zhang, H. (2021). Synergistic enhancement of electrocatalytic nitrogen reduction over boron nitride quantum dots decorated Nb_2CT_x-MXene. Small *17*, 2102363. https://doi.org/10.1002/smll.202102363.

8. Liu, C., Li, S., Li, Z., Zhang, L., Chen, H., Zhao, D., Sun, S., Luo, Y., Alshehri, A.A., Hamdy, M.S., et al. (2022). Ambient N_2-to-NH_3 fixation over a CeO_2 nanoparticle decorated three-dimensional carbon skeleton. Sustain. Energy Fuels *6*, 3344–3348. https://doi.org/10.1039/D2SE00557C.

9. Cai, X., Fu, C., Iriawan, H., Yang, F., Wu, A., Luo, L., Shen, S., Wei, G., Shao-Horn, Y., and Zhang, J. (2021). Lithium-mediated electrochemical nitrogen reduction: mechanistic insights to enhance performance. iScience *24*, 103105. https://doi.org/10.1016/j.isci.2021.103105.

10. Luo, Y., Li, Q., Tian, Y., Liu, Y., and Chu, K. (2022). Amorphization engineered VSe_{2-x} nanosheets with abundant Se-vacancies for enhanced N_2 electroreduction. J. Mater. Chem. *10*, 1742–1749. https://doi.org/10.1039/D1TA06746J.

11. Sun, Y., Wu, W., Yu, L., Xu, S., Zhang, Y., Yu, L., Xia, B., Ding, S., Li, M., Jiang, L., et al. (2022). Asymmetric acidic/alkaline N_2 electrofixation accelerated by high-entropy metal-organic framework derivatives. Carbon Energy *5*, e263. https://doi.org/10.1002/cey2.263.

12. Ren, Y., Yu, C., Tan, X., Huang, H., Wei, Q., and Qiu, J. (2021). Strategies to suppress hydrogen evolution for highly selective electro catalytic nitrogen reduction: challenges and perspectives. Energy Environ. Sci. *14*, 1176–1193. https://doi.org/10.1039/D0EE03596C.

13. Li, L., Tang, C., Jin, H., Davey, K., and Qiao, S.Z. (2021). Main-group elements boost electrochemical nitrogen fixation. Chem *7*, 3232–3255. https://doi.org/10.1016/j.chempr.2021.10.008.

14. Zhao, C., Xi, M., Huo, J., He, C., and Fu, L. (2022). Electro-reduction of N_2 on nanostructured materials and the design strategies of advanced catalysts based on descriptors. Mater. Today Phys. *22*, 100609. https://doi.org/10.1016/j.mtphys.2022.100609.

15. Shen, P., Li, X., Luo, Y., Guo, Y., Zhao, X., and Chu, K. (2022). High-efficiency N_2 electroreduction enabled by Se-vacancy-rich WSe_{2-x} in water-in-salt electrolytes. ACS Nano *16*, 7915–7925. https://doi.org/10.1021/acsnano.2c00596.

16. Yao, D., Tang, C., Li, L., Xia, B., Vasileff, A., Jin, H., Zhang, Y., and Qiao, S. (2020). In situ fragmented bismuth nanoparticles for electrocatalytic nitrogen reduction. Adv. Energy Mater. *10*, 2001289. https://doi.org/10.1002/aenm.202001289.

17. Zhao, X., Hu, G., Chen, G.-F., Zhang, H., Zhang, S., and Wang, H. (2021). Comprehensive understanding of the thriving ambient electrochemical nitrogen reduction reaction. Adv. Mater. *33*, 2007650. https://doi.org/10.1002/adma.202007650.

18. Chanda, D., Xing, R., Xu, T., Liu, Q., Luo, Y., Liu, S., Tufa, R.A., Dolla, T.H., Montini, T., and Sun, X. (2021). Electrochemical nitrogen reduction: recent progress and prospects. Chem. Commun. *57*, 7335–7349. https://doi.org/10.1039/D1CC01451J.

19. Li, S., Liang, J., Wei, P., Liu, Q., Xie, L., Luo, Y., and Sun, X. (2022). ITO@TiO_2 nanoarray: an efficient and robust nitrite reduction reaction electrocatalyst toward NH_3 production under ambient conditions. eScience *2*, 382–388. https://doi.org/10.1016/j.esci.2022.04.008.

20. Li, H., Yan, C., Guo, H., Shin, K., Humphrey, S.M., Werth, C.J., and Henkelman, G. (2020). Cu_xIr_{1-x} nanoalloy catalysts achieve near 100% selectivity for aqueous nitrite reduction to NH_3. ACS Catal. *10*, 7915–7921. https://doi.org/10.1021/acscatal.0c01604.

21. Galloway, J.N., Townsend, A.R., Erisman, J.W., Bekunda, M., Cai, Z., Freney, J.R., Martinelll, L.A., Seitzinger, S.P., and Sutton, M.A. (2008). Transformation of the nitrogen cycle: recent trends, questions, and potential solutions. Science *320*, 889–892. https://doi.org/10.1126/science.1136674.

22. Kanter, D.R., Chodos, O., Nordland, O., Rutigliano, M., and Winiwarter, W. (2020). Gaps and opportunities in nitrogen pollution policies around the world. Nat. Sustain. *3*, 956–963. https://doi.org/10.1038/s41893-020-0577-7.

23. He, X., Li, X., Fan, X., Li, J., Zhao, D., Zhang, L., Sun, S., Luo, Y., Zheng, D., Xie, L., et al. (2022). Ambient electroreduction of nitrite to ammonia over Ni nanoparticle supported on molasses-derived carbon sheets. ACS Appl. Nano Mater. *5*, 14246–14250. https://doi.org/10.1021/acsanm.2c03720.

24. Braley, S.E., Xie, J., Losovyj, Y., and Smith, J.M. (2021). Graphite conjugation of a macrocyclic cobalt complex enhances nitrite electroreduction to ammonia. J. Am. Chem. Soc. *143*, 7203–7208. https://doi.org/10.1021/jacs.1c03427.

25. Figueiredo, M.C., Climent, V., and Feliu, J.M. (2011). Nitrite reduction on bismuth modified Pt (111) surfaces in different electrolytic media. Electrocatalysis *2*, 2255–2262. https://doi.org/10.1007/s12678-011-0053-2.

26. Li, H., Guo, S., Shin, K., Wong, M.S., and Henkelman, G. (2019). Design of a Pd-Au nitrite reduction catalyst by identifying and optimizing active ensembles. ACS Catal. *9*, 7957–7966. https://doi.org/10.1021/acscatal.9b02182.

27. Troutman, J.P., Li, H., Haddix, A.M., Kienzle, B.A., Henkelman, G., Humphrey, S.M., and Werth, C.J. (2020). PdAg alloy nanocatalysts: toward economically viable nitrite reduction in drinking water. ACS Catal. *10*, 7979–7989. https://doi.org/10.1021/acscatal.0c01538.

28. Liu, Q., Wen, G., Zhao, D., Xie, L., Sun, S., Zhang, L., Luo, Y., Ali Alshehri, A., Hamdy, M.S., and Kong, Q. (2022). Nitrite reduction over Ag nanoarray electrocatalyst for ammonia synthesis. J. Colloid Interface Sci. *623*, 513–519. https://doi.org/10.1016/j.jcis.2022.04.173.

29. Mattarozzi, L., Cattarin, S., Comisso, N., Guerriero, P., Musiani, M., Vázquez-Gómez, L., and Verlato, E. (2013). Electrochemical reduction of nitrate and nitrite in alkaline media at CuNi alloy electrodes. Electrochim.

Acta *89*, 488–496. https://doi.org/10.1016/j.electacta.2012.11.074.

30. Li, X., He, X., Yao, J., Dong, K., Hu, L., Chen, J., Zhang, L., Fan, X., Cai, Z., Sun, S., et al. (2023). High-efficiency electroreduction of nitrite to ammonia on Ni nanoparticles strutted 3D honeycomb-like porous carbon framework. ChemSusChem, e202300505. https://doi.org/10.1002/cssc.202300505.

31. Wang, C., Zhou, W., Sun, Z., Wang, Y., Zhang, B., and Yu, Y. (2021). Integrated selective nitrite reduction to ammonia with tetrahydroisoquinoline semi-dehydrogenation over a vacancy-rich Ni bifunctional electrode. J. Mater. Chem. *9*, 239–243. https://doi.org/10.1039/D0TA09590G.

32. He, X., Hu, L., Xie, L., Li, Z., Chen, J., Li, X., Li, J., Zhang, L., Fang, X., Zheng, D., et al. (2023). Ambient ammonia synthesis via nitrite electroreduction over NiS_2 nanoparticles-decorated TiO_2 nanoribbon array. J. Colloid Interface Sci. *634*, 86–92. https://doi.org/10.1016/j.jcis.2022.12.042.

33. Guo, Y., Stroka, J.R., Kandemir, B., Dickerson, C.E., and Bren, K.L. (2018). Cobalt metallopeptide electrocatalyst for the selective reduction of nitrite to ammonium. J. Am. Chem. Soc. *140*, 16888–16892. https://doi.org/10.1021/jacs.8b09612.

34. Zhang, R., Zhang, S., Guo, Y., Li, C., Liu, J., Huang, Z., Zhao, Y., Li, Y., and Zhi, C. (2022). A Zn–nitrite battery as an energy-output electrocatalytic system for high-efficiency ammonia synthesis using carbon-doped cobalt oxide nanotubes. Energy Environ. Sci. *15*, 3024–3032. https://doi.org/10.1039/D2EE00686C.

35. Yi, L., Shao, P., Li, H., Zhang, M., Peng, X., Chen, K., Liu, X., and Wen, Z. (2023). Scalable synthesis of MoS_2 nanosheets electrocatalyst towards high-efficiency nitrite reduction to ammonia. J. Power Sources *559*, 232668. https://doi.org/10.1016/j.jpowsour.2023.232668.

36. Tian, J., Liu, Q., Asiri, A.M., and Sun, X. (2014). Self-supported nanoporous cobalt phosphide nanowire arrays: an efficient 3D hydrogen-evolving cathode over the wide range of pH 0–14. J. Am. Chem. Soc. *136*, 7587–7590. https://doi.org/10.1021/ja503372r.

37. Ji, L., Wang, J., Teng, X., Meyer, T.J., and Chen, Z. (2019). CoP nanoframes as bifunctional electrocatalysts for efficient overall water splitting. ACS Catal. *10*, 412–419. https://doi.org/10.1021/acscatal.9b03623.

38. Wen, G., Liang, J., Liu, Q., Li, T., An, X., Zhang, F., Alshehri, A.A., Alzahrani, K.A., Luo, Y., Kong, Q., et al. (2022). Ambient ammonia production via electrocatalytic nitrite reduction catalyzed by a CoP nanoarray. Nano Res. *15*, 972–977. https://doi.org/10.1007/s12274-021-3583-9.

39. Zhang, H., Wang, G., Wang, C., Liu, Y., Yang, Y., Wang, C., Jiang, W., Fu, L., and Xu, J. (2022). CoP nanowires on carbon cloth for electrocatalytic NO_x^- reduction to ammonia. J. Electroanal. Chem. *910*, 116171. https://doi.org/10.1016/j.jelechem.2022.116171.

40. Cisneros, S., Abdel-Mageed, A., Mosrati, J., Bartling, S., Rockstroh, N., Atia, H., Abed, H., Rabeah, J., and Brückner, A. (2022). Oxygen vacancies in Ru/TiO_2-drivers of low-temperature CO_2 methanation assessed by multimodal operando spectroscopy. iScience *25*, 103886. https://doi.org/10.1016/j.isci.2022.103886.

41. Gao, J., Jiang, B., Ni, C., Qi, Y., Zhang, Y., Oturan, N., and Oturan, M.A. (2019). Non-precious Co_3O_4-TiO_2/Ti cathode based electrocatalytic nitrate reduction: preparation, performance and mechanism. Appl. Catal. B Environ. *254*, 391–402. https://doi.org/10.1016/j.apcatb.2019.05.016.

42. Wu, L., Zheng, J., Wang, L., Xiong, X., Shao, Y., Wang, G., Wang, J.-H., Zhong, S., and Wu, M. (2019). PPy-encapsulated SnS_2 nanosheets stabilized by defects on a TiO_2 support as a durable anode material for lithium-ion batteries. Angew. Chem. Int. Ed. Engl. *131*, 821–825. https://doi.org/10.1002/ange.201811784.

43. Fan, X., Ma, C., Zhao, D., Deng, Z., Zhang, L., Wang, Y., Luo, Y., Zheng, D., Li, T., Zhang, J., et al. (2023). Unveiling selective nitrate reduction to ammonia with Co_3O_4 nanosheets/TiO_2 nanobelt heterostructure catalyst. J. Colloid Interface Sci. *630*, 714–720. https://doi.org/10.1016/j.jcis.2022.10.050.

44. Ouyang, L., He, X., Sun, S., Luo, Y., Zheng, D., Chen, J., Li, Y., Lin, Y., Liu, Q., Asiri, A.M., et al. (2022). Enhanced electrocatalytic nitrite reduction to ammonia over P-doped TiO_2 nanobelt array. J. Mater. Chem. *10*, 23494–23498. https://doi.org/10.1039/D2TA06933D.

45. Wang, H., Zhang, F., Jin, M., Zhao, D., Fan, X., Li, Z., Luo, Y., Zheng, D., Li, T., Wang, Y., et al. (2023). V-doped TiO_2 nanobelt array for high-efficiency electrocatalytic nitrite reduction to ammonia. Mater. Today Phys. *30*, 100944. https://doi.org/10.1016/j.mtphys.2022.100944.

46. Liu, B., Cao, B., Cheng, Y., Jing, P., Zhao, J., Gao, R., O'Mullane, A., Zhu, H., Liu, K., Sun, X., et al. (2020). Ultrafine CoP/Co_2P nanorods encapsulated in janus/twins-type honeycomb 3D nitrogen-doped carbon nanosheets for efficient hydrogen evolution. iScience *23*, 101264. https://doi.org/10.1016/j.isci.2020.101264.

47. Liang, J., Hu, W.F., Song, B., Mou, T., Zhang, L., Luo, Y., Liu, Q., Alshehri, A.A., Hamdy, M.S., Yang, L.-M., et al. (2022). Efficient nitric oxide electroreduction toward ambient ammonia synthesis catalyzed by a CoP nanoarray. Inorg. Chem. Front. *9*, 1366–1372. https://doi.org/10.1039/d2qi00002.

48. He, X., Li, J., Li, R., Zhao, D., Zhang, L., Ji, X., Fan, X., Chen, J., Wang, Y., Luo, Y., et al. (2023). Ambient ammonia synthesis via nitrate electroreduction in neutral media on Fe_3O_4 nanoparticles-decorated TiO_2 nanoribbon array. Inorg. Chem. *62*, 25–29. https://doi.org/10.1021/acs.inorgchem.2c03640.

49. Nabi, I., Bacha, A.-U.-R., Li, K., Cheng, H., Wang, T., Liu, Y., Ajmal, S., Yang, Y., Feng, Y., and Zhang, L. (2020). Complete Photocatalytic Mineralization of Microplastic on TiO_2 Nanoparticle Film. iScience *23*, 101326. https://doi.org/10.1016/j.isci.2020.101326.

50. Wang, H., Si, J., Zhang, T., Li, Y., Yang, B., Li, Z., Chen, J., Wen, Z., Yuan, C., et al. (2020). Exfoliated metallic niobium disulfate nanosheets for enhanced electrochemical ammonia synthesis and Zn-N_2 battery. Appl. Catal. B Environ. *270*, 118892. https://doi.org/10.1016/j.apcatb.2020.118892.

51. Lv, X.W., Liu, Y., Wang, Y.S., Liu, X.L., and Yuan, Z.Y. (2021). Encapsulating vanadium nitride nanodots into N, S-codoped graphitized carbon for synergistic electrocatalytic nitrogen reduction and aqueous Zn-N_2 battery. Appl. Catal. B Environ. *280*, 119434. https://doi.org/10.1016/j.apcatb.2020.119434.

52. Guo, Y., Zhang, R., Zhang, S., Zhao, Y., Yang, Q., Huang, Z., Dong, B., and Zhi, C. (2021). Pd doping-weakened Intermediate adsorption to promote electrocatalytic nitrate reduction on TiO_2 nanoarrays for ammonia production and energy supply with Zinc-nitrate batteries. Energy Environ. Sci. *14*, 3938–3944. https://doi.org/10.1039/D1EE00806D.

STAR★METHODS

KEY RESOURCES TABLE

REAGENT or RESOURCE	SOURCE	IDENTIFIER
Chemicals, peptides, and recombinant proteins		
$Co(NO_3)_2 \cdot 6H_2O$	Aladdin Co., Ltd.	10026-22-9
NaH_2PO_2	Aladdin Co., Ltd.	7681-53-0
$NaNO_2$	Aladdin Co., Ltd.	7632-00-0
NH_4Cl	Aladdin Co., Ltd.	12125-02-9
NaOH	Aladdin Co., Ltd.	1310-73-2
$C_7H_5NaO_3$	Aladdin Co., Ltd.	54-21-7
$C_6H_5Na_3O_7 \cdot 2H_2O$	Aladdin Co., Ltd.	6132-04-3
$C_9H_{11}NO$	Aladdin Co., Ltd.	100-10-7
$C_5FeN_6Na_2O \cdot 2H_2O$	Aladdin Co., Ltd.	13755-38-9
NaClO	Aladdin Co., Ltd.	7681-52-9
H_2SO_4	Beijing Chemical Corporation	7664-93-9
H_2O_2	Beijing Chemical Corporation	7722-84-1
$N_2H_4 \cdot H_2O$	Beijing Chemical Corporation	7803-57-8
HCl	Beijing Chemical Corporation	7647-01-0
C_2H_5OH	Beijing Chemical Corporation	64-17-5
Ti plate	Qingyuan Metal Materials Co., Ltd.	/

RESOURCE AVAILABILITY

Lead contact

Further information and requests for resources should be directed to and will be fulfilled by the lead contact, Dr. Xuping Sun (xpsun@uestc.edu.cn).

Materials availability

This study did not generate new unique reagents. All chemicals were obtained from commercial resources and used as received.

Data and code availability

- Data reported in this paper will be shared by the lead contact upon reasonable request.
- This study does not report any original code.
- Any additional information required to reanalyze the data reported in this paper is available from the lead contact upon reasonable request.

METHOD DETAILS

Synthesis of CoP@TiO_2/TP

To synthesize CoP@TiO_2/TP, many pieces TP measuring 2.0 × 3.0 cm^2 were sonicated in HCl, C_2H_5OH, and water for 10 min each. The pretreated TP were then placed in a Teflon-lined autoclave containing 5 M NaOH solutions and heated at 180°C for 24 h to obtain $Na_2Ti_2O_5$/TP. The resulting $Na_2Ti_2O_5$/TP was then immersed in 0.1 M $Co(NO_3)_2$ for 1 h to replace Na^+ with Co^{2+}. After washing with water and drying, the obtained $CoTi_2O_5$/TP was annealed with NaH_2PO_2 at 500°C for 1 h under an Ar atmosphere, resulting in the final product, CoP@TiO_2/TP. For comparison, TiO_2/TP was also synthesized using the same process as CoP@TiO_2/TP, but the $Na_2Ti_2O_5$/TP was immersed in diluted HCl to exchange Na^+ to H^+.

Characterizations

X-ray diffractometer (XRD) loaded a Cu Kα radiation target (40 kV, 30 mA) (SHIMADZU, Japan), scanning electron microscope (SEM) with 5 kV acceleration voltage (ZEISS, Germany), transmission electron microscopy (TEM) with a Zeiss Libra 200FE, and X-ray photoelectron spectroscopy (XPS) (ESCALAB 250 Xi) were applied to study the composition and morphology of the prepared CoP@TiO_2 and TiO_2. Gas chromatography (GC) (Shimadzu GC-2014C) was used to detect gaseous products. Ultraviolet-visible spectrophotometer (UV–vis) was applied to measure absorbance (SHIMADZU UV-1800).

Electrochemical measurements

Electrochemical tests were conducted in a H-type cell separated by a Nafion 117 membrane using a CHI 760E electrochemical workstation (Shanghai, Chenhua). The electrolyte solution (30 mL) was Ar-saturated 0.1 M NaOH with and without NO_2^- ($NaNO_2$), with CoP@TiO_2/TP (0.5 × 0.5 cm^2), graphite rod, and Hg/HgO as the working electrode, counter electrode, and reference electrode, respectively. To conform to the Nernst equation, all potentials were converted into the potential of the reversible hydrogen electrode (RHE) ($E_{RHE} = E_{Hg/HgO} + 0.059 \times pH + 0.098$ V). Linear sweep voltammetry (LSV) curves were tested using the CHI 760E with a scan rate of 5 mV^{-1}.

To determine the NH_3 concentration in the solution, colorimetry was used (the obtained electrolyte was diluted 40 times) via the indophenol blue method. Specifically, 2 mL of the solution after the reaction was mixed with 2 mL of 1 M NaOH coloring solution containing 5% $C_7H_5NaO_3$ and 5% $C_6H_5Na_3O_7 \cdot 2H_2O$. Then, 1 mL of oxidizing solution of 0.05 M NaClO and 0.2 mL of catalyst solution of $C_5FeN_6Na_2O$ (1 wt%) were added to the above solution. After standing in the dark for 2h, the UV–vis absorption spectra were measured, and the NH_3 concentration was identified using the absorbance at a wavelength of 655 nm. The concentration-absorbance curve was calibrated using the standard NH_4Cl solution with NH_3 concentrations of 0, 0.2, 0.5, 1.0, 2.0, and 5.0 ppm in 0.1 M NaOH solution. The fitting curve (0.3541 x+0.00875, R^2=0.9993) showed a good linear relation of absorbance value with NH_3 concentration.

To estimate N_2H_4, the Watt and Crisp method was used. The color reagent was a solution of 18.15 mg/mL of $C_9H_{11}NO$ in the mixed solvent of HCl and C_2H_5OH (V/V: 1/10). In detail, 2 mL of electrolyte was added to 2 mL of the color reagent for 15 min under stirring. The absorbance of such solution was measured to quantify the hydrazine yields by the standard curve of hydrazine (y = 0.68479 x + 0.10146, R^2=0.9993).

Determination of NH_3 yield and FE:

$$FE = \frac{nCVF}{MQ}$$

$$NH_3\ yield = \frac{CV}{17tA}$$

Here, n represents the number of electrons transferred during NO_2^-RR, C represents the concentration of products, V represents the volume of the cathodic electrolyte (35 mL), F is the Faradaic constant (96500 C mol^{-1}), M is the molar mass of products, Q is the total quantity of applied electricity, t is the electrolysis time, and A is the geometric area of the working electrode (0.5 × 0.5 cm^2). The partial current densities in Figure S11, one can multiply the average current density at each potential with the FE of each reduction product.